*This document is the preprint version of the final paper:*
*Abusara, M.A.; Guerrero, J.M.; Sharkh, S.M., "Line Interactive UPS for Microgrids," Industrial Electronics, IEEE Transactions on , 2013, Early access. doi: 10.1109/TIE.2013.2262763*
*keywords: {Line interactive UPS; distributed generation; microgrid},*
*URL:* http://ieeexplore.ieee.org/stamp/stamp.jsp?tp=&arnumber=6515659&isnumber=4387790

# Line Interactive UPS for Microgrids

Mohammad A. Abusara, Josep M. Guerrero, *Senior Member, IEEE*, and Suleiman M. Sharkh

***Abstract*— Line interactive Uninterruptable Power Supply (UPS) systems are good candidates for providing energy storage within a microgrid to help improve its reliability, economy and efficiency. In grid-connected mode, power can be imported from the grid by the UPS to charge its battery. Power can also be exported when required, e.g., when the tariffs are advantageous. In stand-alone mode, the UPS supplies local distributed loads in parallel with other sources. In this paper, a line interactive UPS and its control system are presented and discussed. Power flow is controlled using the frequency and voltage drooping technique to ensure seamless transfer between grid-connected and stand-alone parallel modes of operation. The drooping coefficients are chosen to limit the energy imported by the USP when re-connecting to the grid and to give good transient response. Experimental results of a microgrid consisting of two 60kW line interactive UPS systems are provided to validate the design.**

***Index Terms*—Line interactive UPS, microgird, distributed generation.**

## I. Introduction

To increase reliability, energy storage systems within a microgrid are essential. Energy is stored while in grid-connected mode, when the microgrid's Distributed Generation (DG) systems produce excess power, to be used later to supply critical loads during power outages. In stand-alone mode, they can be used to boost the power supplied by the microgrid if the DG systems cannot meet the expected level of power. To meet these demands, the energy storage system needs to be able to work in grid-connected and stand-alone modes. In the latter mode of operation, the system needs to operate in parallel with other DG systems to meet the variable power demand of the load. More importantly, it needs to switch seamlessly between the two modes.

Line interactive UPS systems are good candidates for providing energy storage within microgrids as they can be connected in parallel with both the main grid and local load. The classical topology of line interactive UPS systems [1],[2] is simpler, cheaper, more efficient and more reliable than the on-line double conversion UPS. This topology, however, does not provide voltage regulation to the load. Voltage regulation is possible as in series-parallel or delta conversion line-interactive UPS [3]-[6] at the expense of lower efficiency and extra size and cost due to the use of extra inverter and bulky transformer. However, this topology is still more efficient than classical on-line double conversion UPS because the complementary inverter has only to supply 10% to 20% of the UPS nominal power [7].

There are a number of publications on the control of line interactive UPS systems [8]-[15]. Tirumala et al. [8] proposed a control algorithm for grid interactive PWM inverters to obtain a seamless transfer from grid-connected mode to stand-alone mode and vice versa. When it is connected to the grid, the inverter operates in current-controlled mode regulating the current injected into the point of common coupling (PCC). In stand-alone mode, however, the inverter operates in voltage-controlled mode regulating the output voltage across the load. Similar approaches were also reported in [9] and [10]. The main disadvantage of these systems is that the load voltage after the grid fails and before starting the transitional period (from current-controlled to voltage controlled mode) depends on the current demand and the load. This might result in a very high or very low voltage across the load during the transitional period. A notch filler that is used to mitigate these voltage transients was proposed in [11]. Kim et al. [12] proposed a controller for truly seamless transfer from grid-connected mode to stand-alone mode. The controller has an inner voltage control loop that regulates the output voltage. During grid-connection, the power angle (the angle between the inverter voltage and the voltage at the PCC) of the output voltage is set by an outer control loop depending on the required injected grid current. When the grid fails, the power angle is saturated to a maximum pre-defined value. In the system reported in [13], the power angle between the UPS voltage and the grid voltage is measured by a phase detector and adjusted to control the power. The line interactive UPS system proposed in [14] has the voltage controller and the current controller working in parallel in order to achieve seamless transfer between the two modes. Although the controllers reported above enable seamless transfer of a single unit from grid-connected and stand-alone mode, the main disadvantage is that the UPS units are not capable of operating autonomously in parallel with other DG units and thus they cannot form a microgrid.

Chandorkar et al. [15] proposed a line interactive UPS system based on $P$-$\omega$ and $Q$-$V$ droop control where the inverter frequency and voltage amplitude are drooped linearly with the inverter output active and reactive power, respectively. UPS units can operate in parallel and load sharing is achieved without the need for communication signals between the

M. A. Abusara was with Bowman Power Group, UK and now he is with the Renewable Energy Research Group, University of Exeter, Cornwall Campus, Penryn, TR10 9EZ, U.K. (e-mail: m.abusara@exeter.ac.uk).

J. M. Guerrero is with the Department of Energy Technology, Aalborg University, 9220 Aalborg, Denmark (e-mail: joz@et.aau.dk).

S. M. Sharkh is with the Electro-Mechanical Engineering Research Group, University of Southampton, Highfield Campus, Southampton, SO17 1BJ, U.K. (e-mail: suleiman@soton.ac.uk).

inverters. In [16], a line interactive UPS system that is capable of operating in a microgrid was proposed. The controller of the UPS inverter is based on two control loops: an inner voltage feedback loop that regulates the output voltage and an outer active and reactive power sharing loop which is implemented by drooping control. Both systems in [15], [16] provide truly seamless transfer between grid-connected mode and stand-alone parallel mode and vice versa. However, the integration of the battery and its DC/DC converter into the system was not studied. Also, the stability of the DC-link voltage was not discussed. This becomes an important issue, taken into the account the requirement to transfer seamlessly from battery charging mode in grid-connected mode to battery discharging in stand-alone paralleling mode.

This paper presents and discusses a line interactive UPS system to be used within a microgrid as illustrated in Fig. 1. The system can transfer practically seamlessly between grid-connected and stand-alone modes sharing the load within a microgrid in parallel with other DG units. The control of the complete system including the battery and its bidirectional DC/DC converter is considered. The main novel contributions of the paper are: 1) Analysis, design and experimental implementation of a new control strategy of a line interactive UPS system within a microgrid which enables seamless transfer between grid-connected and stand-alone parallel modes of operation, 2) The design of a DC-link controller loop that sets the active power demand during battery charging mode which allows for a smooth transition between battery charging and discharging modes.

## II. System Overview

The general overall structure of a microgrid (Fig. 1) consists of DG units, UPS units, local loads, supervisory controller, and a static transfer switch (STS). The STS is used at the PCC to isolate the microgrid from the grid in case of grid faults and reconnect seamlessly to the grid when the faults are cleared. Local loads are connected on the microgrid side of the switch so that they are always supplied with electrical power regardless of the status of the switch. The controller of each DG system uses local measurements of voltage and current to control the output voltage and power flow. There is still however a need for low speed communication between the STS and the DG units to update them about the status of the switch, i.e., whether it is opened or closed. Furthermore, the supervisory controller measures the power at the PCC, receives information about the state of charge (SOC) of the batteries from the UPS controllers and sends active and reactive power commands $P_{ref}$ and $Q_{ref}$ to the other DG units based on tariffs, local load requirements, and efficiency of the units.

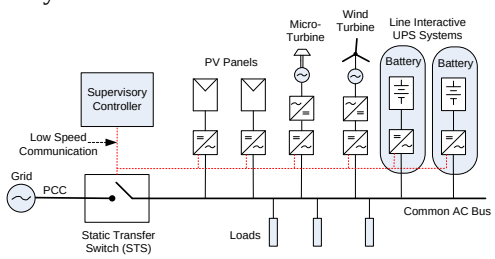


Fig. 1. Microgrid structure.

When the grid is connected, the UPS can export power to the grid or it can import power to charge their batteries. For example, the supervisory controller may charge the battery during the grid off-peak tariff and discharge it during peak tariff periods. When a grid fault occurs, the anti-islanding controllers embedded inside the controllers of the DG units push the voltage amplitude and/or frequency at the PCC toward their upper or lower limits. Once the amplitude or frequency upper or lower limits are reached, the controller of the STS decides that the grid is not healthy and opens the switch. It also sends a signal to the DG units to update them about the status of the switch. The DG units carry on supplying power in parallel according to their ratings, sharing the power demanded by the distributed local loads. After the grid fault is cleared, the STS reconnects the microgrid: it monitors the voltage signals on both sides and closes when these signals are in phase to ensure transient free operation.

The microgrid considered in this paper consists of two 60kW line interactive UPS systems each powered by a 30Ah (550 -700 V) lithium-ion battery. The circuit diagram of each UPS system is shown in Fig. 2. The UPS system consists of a battery, a bidirectional DC/DC converter [17], and a bidirectional three-phase DC/AC converter with an output *LCL* filter. The DC/AC converter parameters are given in Table I. When the power flows from the grid to the battery, the DC/DC converter operates in buck mode and the boost IGBT is held open. When the power flows in the opposite direction, the buck IGBT is held open and the DC/DC converter operates in boost mode regulating the DC-link voltage to a suitable level in order to inject power into the grid. Fig. 3 shows the controller of the bidirectional DC/AC converter. An outer power flow controller sets the voltage demand for an inner voltage core controller loop. The core voltage controller (not shown) regulates the capacitor voltage $V_c$. The response time for the inner core controller is much faster than the outer power flow loop and hence it will be assumed (from the point of view of the power flow controller) as an ideal voltage source with settable magnitude and frequency. Fig. 4 shows the controller of the bidirectional DC/DC converter. During battery charging mode, the Buck IGBT is pulse width modulated and, depending on the battery voltage, the controller operates either in current mode or voltage mode regulating the battery current or voltage, respectively. When the battery discharges, the boost IGBT is modulated to regulate the DC-link voltage. During battery charging, the DC-link voltage is controlled by the three-phase DC/AC converter, which in this case operates as an active rectifier. When discharging, however, the DC-link voltage is controlled by the DC/DC converter, operating in boost mode as mentioned earlier. To decouple these two controllers, which control a common DC-link voltage, the voltage demand for the active rectifier $V^*_{dclink\_2}$ is set to be higher (800 V) than the voltage demand of the boost $V^*_{dclink\_1}$ (750 V). To understand how the controllers react during a sudden transition between operating modes, the following scenario is considered. Suppose that the UPS is in charging mode, the DC-link in this case will be regulated by the DC/AC converter operating as an active rectifier and the DC/DC converter will be charging the battery in buck mode.

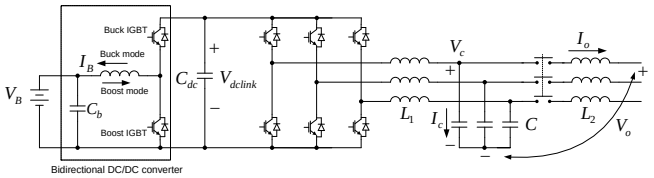

Fig. 2. Circuit diagram of the UPS system

TABLE I
DC/AC CONVERTER PARAMETER VALUES

| Symbol | Value | Description |
|---|---|---|
| $L_1$ | 350μH | Inverter-side filter inductor |
| $C$ | 160μF | Filter capacitor |
| $L_2$ | 250μH | Grid-side filter inductor |
| $C_{dc}$ | 2000μF | DC link capacitor |
| $P_{\max}$ | 60kW | Maximum active power rating |
| $Q_{\max}$ | 45kVAR | Maximum reactive power rating |
| $V_{dclink\_\max}$ | 1000 V | Maximum allowed transient value of the DC-link voltage (trip limit) |

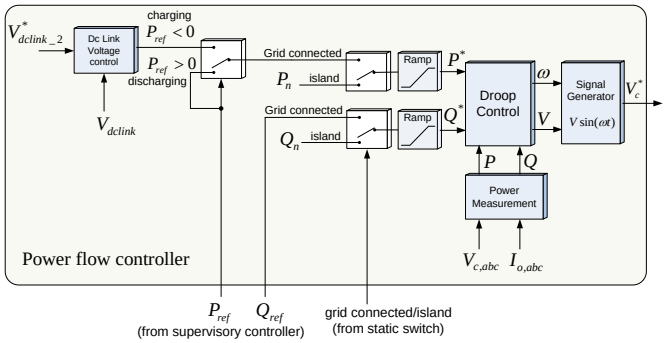

Fig. 3. DC/AC controller

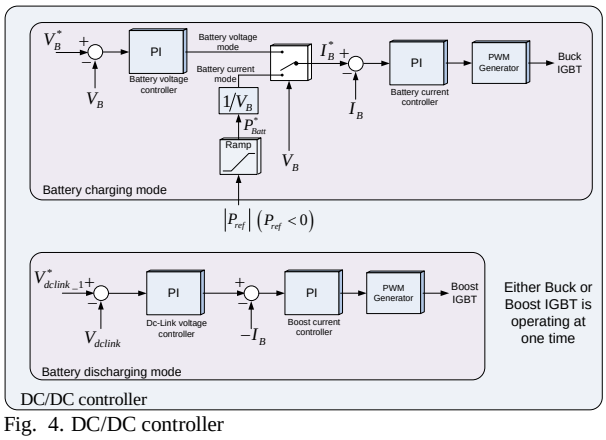

Fig. 4. DC/DC controller

At the moment when the grid fails and before the fault is detected by the STS, the power flow through the three-phase converter changes direction immediately and automatically as a consequence of losing stiffness at the PCC. Thus the power starts to flow from the DC-link capacitor to the AC load causing the DC-link voltage to drop from the $V^*_{dclink\_2}$ demand. Once, the DC-link drops below $V^*_{dclink\_1}$, the DC/DC controller recognizes the event and changes its mode from buck to boost immediately and start regulating the DC-link voltage. In this scheme, the smooth transition from grid connected charging mode to stand-alone mode is possible without relying on external communication. When the grid fault is cleared, the STS closes and sends an update signal to the UPS units. If the power demand received from the supervisory controller during grid-connected mode is positive, i.e., $P_{ref} > 0$, the power flow controller sets the drooping controller demand to $P_{ref}$ such that $P^* = P_{ref}$ as shown in Fig. 3. However, if the power demand from the supervisory controller is negative, i.e., $P_{ref} < 0$, the DC-link voltage controller, within the power flow controller, starts to raise the DC-link voltage to $V^*_{dclink\_2}$. The output of the DC-link voltage controller will be a negative active power demand to the power flow controller. The DC/DC converter will stop operating in boost mode because the DC-link voltage (regulated to $V^*_{dclink\_2}$) is higher than its demand $V^*_{dclink\_1}$. It will then start to operate in buck mode either in current mode or in voltage mode depending on the battery voltage $V_B$. If it operates in current mode, the battery current demand is set to $P^*_{Batt}/V_B$ where $P^*_{Batt}$ is the battery charging power demand and equals to $P^*_{Batt} = \text{Ramp}(|P_{ref}|)$, (the absolute value is used because the $P_{ref}$ in this case is negative). The rate of change of the ramp function needs to be slow enough so it does not disturb the DC-link voltage controller. For instance, if the $P^*_{Batt}$ is changed suddenly, the DC/DC converter will draw a large amount of power from the DC-link capacitor which may result in a drastic drop in the DC-link voltage before the DC-link voltage controller reacts to this drop. To avoid any unnecessary transient, any changes required to $P^*$ and $Q^*$ values in the power flow controller also happen gradually via ramp functions.

## III. POWER FLOW CONTROLLER

### A. Small Signal Analysis

The proposed drooping control is given by

$$\omega = \omega_o^* - \left(k_\omega + k_{\omega\_I}/s\right)(P - P^*) \quad (1)$$

$$V = V_o^* - \left(k_a + k_{a\_I}/s\right)(Q - Q^*) \quad (2)$$

where $\omega_o^*$, $V_o^*$, $k_\omega$, and $k_a$ are the nominal frequency reference, nominal voltage reference, proportional frequency drooping coefficient, and proportional voltage drooping coefficient, respectively. The integral frequency and voltage drooping coefficients $k_{\omega\_I}$, $k_{a\_I}$ are set to zero during island mode but they are activated during grid connected mode to make sure that the power output follows the demand precisely especially when the grid voltage and frequency deviate from their nominal values. The values $P^*$and $Q^*$ are set to the demanded power in grid connected mode. In stand-alone mode, however, they are set to nominal active and reactive power $P_n$ and $Q_n$ to improve frequency and voltage regulation. Because this is a bidirectional UPS system $P_n$ and $Q_n$ are set to zero.

The inverter can be modelled by a two-terminal Thevenin equivalent circuit as shown in Fig. 5(a). $G(s)$ and $Z_o(s)$ represent the closed loop and output impedance transfer functions, respectively [18]. Fig. 5(b) shows an equivalent circuit diagram of the grid-connected UPS unit. $Z_o(s)$ has been replaced by $sL_o$ because the output impedance is predominantly inductive around the fundamental frequency [18]-[20]. The inductance $L_o$ can be determined by the slope of $Z_o(s)$ around the fundamental frequency and it was measured to be 996μH.

The active and reactive power flow between the UPS unit and the grid can be shown to be given by

$$P = 3VV_o \sin\delta / \omega_o L_o \quad (3)$$

$$Q = 3\left(VV_o \cos\delta - V_o^2\right) / \omega_o L_o \quad (4)$$

Small changes in active and reactive power are given by

$$\tilde{P} = \left(3V_o / \omega_o L_o\right)\left(\sin\delta_{eq}.\tilde{V} + V_{eq}\cos\delta_{eq}.\tilde{\delta}\right) \quad (5)$$

$$\tilde{Q} = \left(3V_o / \omega_o L\right)\left(\cos\delta_{eq}.\tilde{V} - V_{eq}\sin\delta_{eq}.\tilde{\delta}\right) \quad (6)$$

where $\delta_{eq}$ and $V_{eq}$ are the equilibrium points around which the small signal analysis is performed. If the equilibrium points are chosen such as $\delta_{eq} = 0$ and $V_{eq} = V_o$, (5) and (6) become

$$\tilde{P} = 3V_o^2\tilde{\delta} / \omega_o L_o \quad (7)$$

$$\tilde{Q} = 3V_o\tilde{V} / \omega_o L_o \quad (8)$$

By perturbing (1) and (2) we get

$$\tilde{\omega} = \tilde{\omega}_o + \left(k_\omega + k_{\omega\_I}/s\right)\left(\tilde{P}^* - \tilde{P}_{meas}\right) \quad (9)$$

$$\tilde{V} = \tilde{V}_o + \left(k_a + k_{a\_I}/s\right)\left(\tilde{Q}^* - \tilde{Q}_{meas}\right) \quad (10)$$

where $\tilde{P}_{meas}$ and $\tilde{Q}_{meas}$ are small changes in the measured active and reactive power, respectively. The grid frequency and voltage reference points $\omega_o^*$ and $V_o^*$ are fixed by the controller. However, the grid frequency $\omega_o$ and voltage $V_o$ may change slightly and hence the notations $\tilde{\omega}_o$ and $\tilde{V}_o$ in (9) and (10) represent the small deviations in the grid frequency and voltage from their nominal values, respectively. The small signal model can be represented by a block diagram as shown in Fig. 6 where the angle $\delta_o$ is the initial angle between the inverter voltage and the common AC bus voltage before connection. It is normally caused by measurement error and it is represented as a disturbance in the block diagram. The transfer function $F(s)$ is the power measurement transfer function that relates the measured power to the actual instantaneous power. Power average can be calculated by integrating the instantaneous power over one fundamental cycle $T$ such as

$$F(s) = \left(1/Ts\right)\left(1 - e^{-Ts}\right) \quad (11)$$

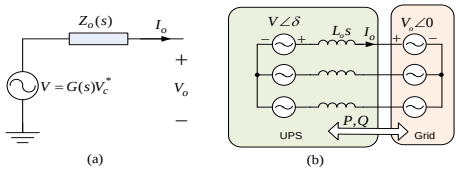


Fig. 5. UPS system equivalent circuit. (a) single phase Thevenin equivalent circuit (b) 3-phase grid connected circuit.

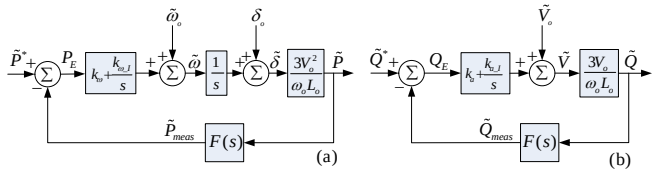


Fig. 6. Small signal model, (a) active power, (b) reactive power

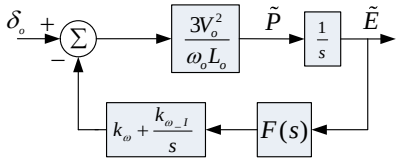


Fig. 7. Block diagram relating $\hat{E}$ to $\delta_o$

TABLE II
TRANSIENT RESPONSE

| $k_\omega$ | $\zeta$ | Energy Overshoot (J) |
|---|---|---|
| $\mathbf{1.0\times10^{-4}}$ | 0.65 | $\mathbf{11000\times\delta_o}$ |
| $\mathbf{1.5\times10^{-4}}$ | 0.44 | $\mathbf{8200\times\delta_o}$ |
| $\mathbf{2.0\times10^{-4}}$ | 0.32 | $\mathbf{7000\times\delta_o}$ |

The time delay in (11) can by replaced by a second order Padé approximation such as

$$e^{-sT} \approx \left(T^2/12s^2 - T/2s + 1\right) / \left(T^2/12s^2 + T/2s + 1\right) \quad (12)$$

Substituting (12) in (11) gives

$$F(s) \approx 1 / \left(T^2/12s^2 + T/2s + 1\right) \quad (13)$$

Equation (13) represents a second order low pass filter with a cutoff frequency of about 140 rad/sec.

### *B. Drooping Coefficients Selection*

The selection of $k_\omega, k_a, k_{\omega\_I}$, and $k_{a\_I}$ will be discussed in this section. The coefficient $k_\omega$ is determined so as to give good dynamic response and at the same time to limit the amount of energy that can be transferred from the AC bus to the UPS unit during grid connection transient. If the angle of the UPS output voltage lags the AC bus voltage by $\delta_o$ when it first connects to the AC bus, active power will flow from the AC bus to the UPS and the energy transferred will cause the DC-link voltage to rise. If the DC-link voltage is higher than the maximum limit $V_{dc\_\max}$, the protection system will trip. Therefore, the objective is to select $k_\omega$ so that the maximum transient energy absorbed by the converter (caused by the presence of an initial power angle $\delta_o$) does not cause the DC-link voltage to rise above the trip limit. If the demand power $\tilde{P}^*$ is set to zero in Fig. 6(a) and by ignoring the disturbance caused by the frequency deviation, the block diagram that relates the output energy (integral of power) to the disturbance $\delta_o$ is shown in Fig. 7. Table II summarizes the results of the damping ratio and the overshoot in the output energy for different values of $k_\omega$. Increasing $k_\omega$ reduces the overshoot in the output energy but also reduces the damping ratio which means that a compromise has to be made. The maximum transient energy that the converter can absorb is given by

$$E_{\max} = 0.5C_{dc}\left(V_{dclink\_\max}^2 - V_{dclink\_o}^2\right) \quad (14)$$

where $V_{dclink\_o}$ is the initial DC-link voltage before transient, $V_{dclink\_max}$ is the maximum allowed DC-link voltage, and $C_{dc}$ is DC-link capacitance. According to the values in Table I and knowing that when the inverter first connects to the AC bus, the initial DC-link voltage is $V_{dclink\_o} = 750\text{V}$, the maximum

energy according to (14) is $E_{\max} = 438$ J. In order to prevent the DC-link voltage from rising to the maximum limit of 1000V, the overshoot transient energy should be less than $E_{\max}$. The initial angle $\delta_o$ depends on the measurement error in the synchronization method (phase locked loop or zero crossing detection). The synchronization in this design is performed by detecting the zero crossing of the AC bus voltage. The error in this case is limited to one sampling period $T_s$ of the AC bus voltage which is for the sampling frequency of 16kHz is equal to 0.02rad. The drooping coefficient is set to $k_\omega = 1.5 \times 10^{-4}$. According to Table II, the maximum energy overshoot is $8200 \times 0.02 = 164$J which is less than $E_{\max}$ calculated above. The damping ratio for the active power controller is 0.44. The voltage amplitude drooping coefficients $k_a$ is set to $k_a = 3 \times 10^{-4}$ which gives a good system damping ratio of 0.6.

The integral drooping coefficients need to be selected so to minimize the effect of any variation in grid frequency and voltage on the output active and reactive power. Because the intention is to minimize the power error resulting from the continuous dynamic deviations in grid frequency and voltage (not only against static deviations), in the analysis to follow, these deviations will be modelled as ramp functions as follows:

$$\tilde{\omega}_o = D_\omega / s^2 \tag{15}$$

$$\tilde{V}_o = D_a / s^2 \tag{16}$$

where $D_\omega$ is the rate of change of the frequency deviation in rad/sec$^2$ and $D_a$ is the rate of change of the voltage deviation in V/sec. From Fig. 6(a), $P_E$ which represents the error signal of the active power is given by

$$P_E = \frac{\left(-3V_o^2/\omega_o L_o\right) s\tilde{\omega}_o}{\frac{T^2}{12}s^4 + \frac{T}{2}s^3 + s^2 + k_\omega \frac{3V_o^2}{\omega_o L_o} s + k_{\omega\_I} \frac{3V_o^2}{\omega_o L_o}} \tag{17}$$

By substituting (15) in (17), the steady state error in active power $P_{E\_ss}$ can be estimated using the final-value theorem:

$$P_{E\_ss} = \lim_{s\to 0}\left(sP_E\right) = -D_\omega / k_{\omega\_I} \tag{18}$$

Similarly, from Fig. 6(b) and (16) the steady state error in reactive power $Q_{E\_ss}$ can be shown to be given by

$$Q_{E\_ss} = \lim_{s\to 0}\left(sQ_E\right) = -D_a / k_{a\_I} \tag{19}$$

The coefficients $k_{\omega\_I}$ and $k_{a\_I}$ are set to $5 \times 10^{-5}$ and $1 \times 10^{-4}$ respectively. It has been found that at the test site, the grid can drift by up to 0.05Hz and 4V in five minutes. This corresponds to $D_\omega = 0.001$ rad/sec$^2$ and $D_a = 0.013$ V/sec. Therefore, according to (18) and (19), the steady state errors in active and reactive power caused by continuous dynamic deviation of the grid frequency and voltage are only $P_{E_ss} = \pm 20$W and $Q_{E_ss} = \pm 130$VAR, respectively.

To validate the small signal model, a detailed model of a three-phase half-bridge PWM inverter with *LCL* filter as per Table I and Table. III was built in Matlab/Simulink. When the inverter connects to the grid, the grid voltage signals were leading the inverter voltage signals (measured at the filter capacitors) by 0.039 rad.

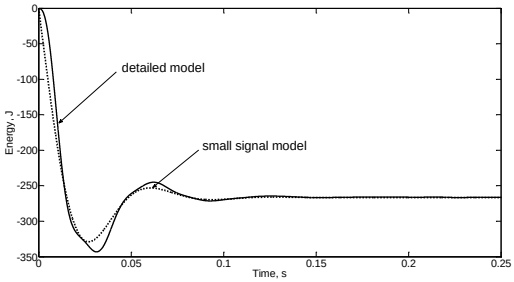


Fig. 8. Energy transient response, actual model and small signal model $\delta_o = 0.039$rad

Fig. 8 shows the response of the inverter transient absorbed energy compared to that of the small signal model produced using Fig. 6(a). It can be seen that the small signal model provides a reasonable prediction of the response of the system in terms of overshoot and frequency of oscillations given the assumptions made to derive the small signal model such as assuming the inverter as an ideal voltage source.

## IV. DC Link Voltage Controller

The DC-link voltage controller regulates the DC-link voltage during battery charging mode. A PI controller is chosen and the overall block diagram of the DC-link voltage controller including the small signal model of the inner loop power flow controller (ignoring the frequency and angle disturbances) is shown in Fig. 9. The power drawn by the DC/DC converter is represented by $\tilde{P}_{Batt}$. It can be noticed that the model is nonlinear due to the presence of the square root function. In order to be able to use linear control design techniques, the square root relation is linearized. Let $x = V_{dclink}^2$, and $y(x) = V_{dclink} = \sqrt{x}$, a small change in $y$ is given by

$$\tilde{y} = \tilde{x}\, dy/dx\big|_{x=x_o} = \tilde{x}\, 0.5/\sqrt{x}\big|_{x=x_o} \tag{20}$$

where $\tilde{x}$ is a small change in $x$, and $x_o$ is the point around which the linearization is performed. Given that the DC-link voltage range of interest is from 750V to 800V, the linearization point is chosen to be $x_o = 775^2$, hence,

$$\tilde{y} = m\tilde{x},\ m = 6.5\times 10^{-4} \tag{21}$$

The open loop transfer function that relates $\tilde{V}_{dclink}$ to $\tilde{P}^*$ (assuming $\tilde{P}_{Batt} = 0$) is therefore given by

$$G_{dc}(s) = \frac{2mA}{C_{dc}}\left(\frac{\left(\left(T^2/12\right)s^2 + \left(T/2\right)s + 1\right)\left(k_\omega s + k_{\omega\_I}\right)}{\left(T^2/12\right)s^5 + \left(T/2\right)s^4 + s^3 + Ak_\omega s^2 + Ak_{\omega\_I}s}\right) \tag{22}$$

where $A = 3V_o^2/\omega_o L_o$.

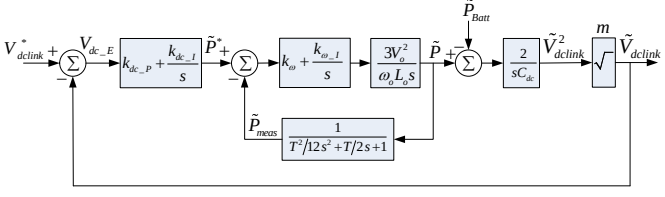


Fig. 9. DC link voltage controller

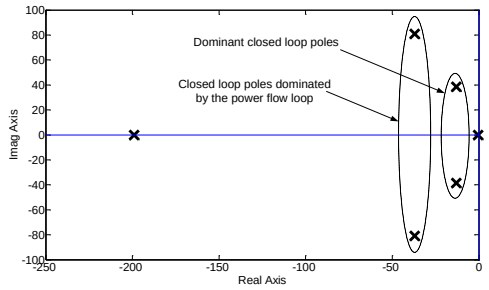


Fig. 10. Closed loop poles of the system

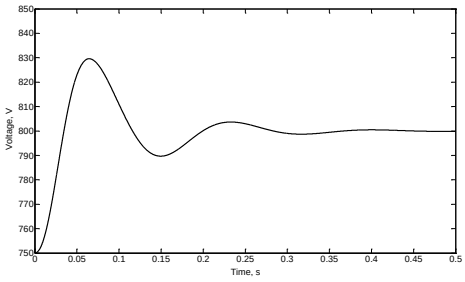


Fig. 11. Step Response of DC link voltage controller.

The design of the DC-link voltage controller now becomes straightforward. The PI gains are chosen so that the dynamic response of the DC-link controller is much slower than the inner power flow controller in order to decouple the two controllers. The proportional and integral gains $k_{dc\_P}$ and $k_{dc\_I}$ are chosen to be 40 and 2000, respectively. Fig. 10 shows the closed loop poles of the complete system. The high frequency poles are the ones caused by the power flow loop whereas the dominant lower frequency poles are caused by DC-link voltage loop. The dynamic of the dominant closed loop poles are well decoupled from the dynamic of the power flow closed loop poles. The simulated response of the controller to step the voltage up from the boost regulated value of 750 V to the active rectifier demand value of 800 V is shown in Fig. 11. The rise and settling times are 0.05sec and 0.3sec, respectively.

The block diagram in Fig. 9 can be used to determine the ramp rate of the power demand sent to the DC/DC (during battery charging mode) to produce $P^*_{Batt}$, (see Fig. 4 ). The ramp rate should be slow enough so it does not cause any major disturbance on the DC-link voltage. For example, if a sudden power is drawn from the DC-link capacitor by the DC/DC converter, the capacitor voltage might drop significantly before the DC-link voltage controller reacts to the disturbance. The power drawn by the DC/DC converter is modelled as a ramp function such as

$$\tilde{P}_{Batt} = D_P / s^2 \tag{23}$$

where $D_P$ is the rate of change in W/sec. From Fig. 9 and by using the final-value theorem, the steady state error in $V_{dclink}$ as a result of the dynamic change in $P^*_{Batt}$ can be shown to be given by

$$V_{dc\_Ess} = \lim_{s\to 0}\left(sV_{dc\_E}\right) = -D_P / k_{dc\_I} \tag{24}$$

The ramp rate $D_P$ is set to 1kW/sec. Therefore, the steady state error caused by ramping up/down the DC/DC power demand is only $V_{dc\_Ess} = \pm 2\text{V}$ .

## V. Experimental Results

A complete microgrid system was built and tested experimentally. The experimental setup is illustrated in Fig. 12. It includes two 60kW line interactive UPS systems and a STS with a supervisory controller. In addition, 60kW resistive load is used as local load. The controller parameters of the converter are shown in Table III. The controllers were implemented using the Texas Instrument TMS320F2812 Fixed point DSP. The low communication link between the STS and the UPS units was realized using Controller Area Network (CAN) protocol. The power demand references were set by the supervisory controller of the STS and sent via CAN bus. Also, for the purpose of testing different scenarios, the power demand could be set by the user via a CAN bus connected computer. An update signal of the status of the STS is also sent to the UPS units via CAN bus.

Fig. 13(a) shows the grid-connected to stand-alone mode transition of one UPS unit. The UPS unit was operating in grid-connected mode charging the battery at 1kw rate (note that the current is 180 deg out of phase with respect to the voltage which means that the UPS is importing power from the grid). A 60 kW local resistive load was also connected to the AC bus and supported by the grid. When the grid fails, the UPS moves seamlessly to stand-alone mode and starts supplying the local load. It can be also observed from the figure that at the moment when the grid fails, the DC-link voltage starts to drop from the active rectifier reference ($V^*_{dclink\_2} = 800V$) due to the change of power flow direction.

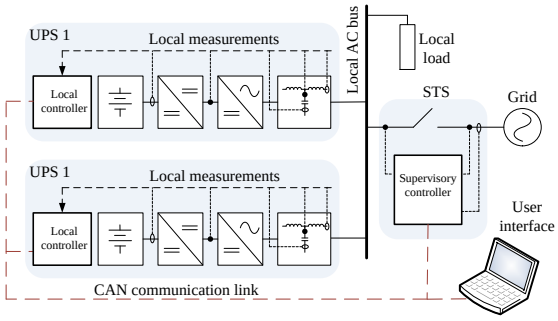


Fig. 12. Experimental setup

TABLE III
CONTROLLER PARAMETER VALUES

| | Value | Description |
|---|---|---|
| $f_{sw}$ | 8kHz | Inverter switching frequency |
| $f_s$ | 16kHz | Voltage controller sampling frequency |
| $k_\omega$ | $1.5 \times 10^{-4}$ | Drooping frequency coefficient |
| $k_a$ | $3.0 \times 10^{-4}$ | Drooping voltage coefficient |
| $k_{\omega\_I}$ | $5.0 \times 10^{-5}$ | Integral drooping frequency coefficient |
| $k_{a\_I}$ | $1.0 \times 10^{-4}$ | Integral Drooping voltage coefficient |
| $\omega^*_o$ | 314.16 rad/sec | Nominal frequency |
| $V^*_o$ | 230 V (rms) | Nominal grid voltage |
| $k_{dc\_P}$ | 40 | DC link voltage controller proportional gain |
| $k_{dc\_I}$ | 2000 | DC link voltage controller (active rectifier) integral gain |
| $V^*_{dclink\_1}$ | 750 V | Boost voltage demand |
| $V^*_{dclink\_2}$ | 800 V | Active rectification demand |

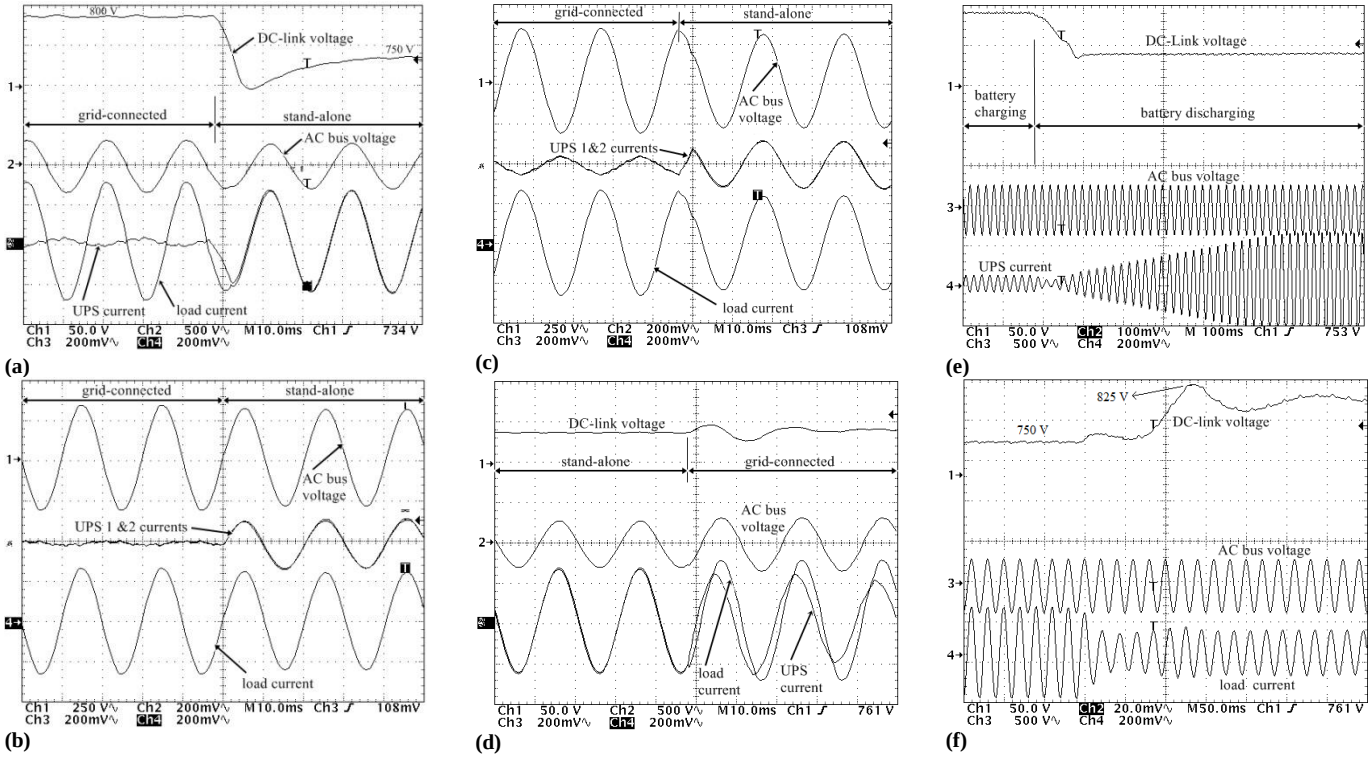


Fig. 13. (current scale: 1A/2mv)

(a) Grid-connected to stand-alone transition of one UPS unit, when in grid connected mode, the UPS was charging the battery at 1kW rate. When in stand-alone mode, the UPS unit was supplying a local 60kW load.

(b) Grid-connected to stand-alone transition of two UPS units, when in grid connected mode, each UPS was producing 0kW. When in stand-alone mode, the two UPS units were sharing a local 60kW load.

(c) Grid-connected to stand-alone transition of two UPS units, when in grid connected mode, each UPS was charging its battery at 10kW rate. When in stand-alone mode, the two UPS units were sharing a local 60kW load.

(d) Stand-alone to grid-connected transition of one UPS units, when in stand-alone mode, the UPS unit was supplying a local 60kW load.

(e) Battery charging (10kW) to discharging (60kW) mode transition.

(f) DC-link voltage controller transient response when going from battery discharging mode (the DC-link voltage is controlled by the DC/DC convertor) to battery charging mode (the DC-link voltage is controlled by the AC/DC converter).

However, when the DC-link drops below the boost reference ($V^*_{dclink\_1} = 750V$) the boost starts to regulate the DC-link voltage and it raises it to 750V. Fig. 13(b) shows the grid-connected to stand-alone mode transition of the two UPS units. Each unit was producing 0kW as both batteries were fully charged. At the moment when the grid fault occurs, the two units move seamlessly to stand-alone parallel mode sharing the 60kW local load equally. The critical load does not see any power interruption as can be seen from the load current signal. The two UPS units behave exactly the same as can be seen from their current signals which are placed on top of each other. In Fig. 13(c), the two UPS units were operating in grid-connected mode charging their batteries at a 10kW rate. When the grid fails, the two inverters move almost seamlessly from grid-connected mode to stand-alone paralleling mode and start sharing the critical load equally. The UPS charging current looks quite distorted and this is because teach unit generates only 17% of its rated power. According to the IEEE Standard 1547 [21], the THD limit is defined based on the unit maximum current, and the distortion at low power is therefore acceptable.

Fig. 13(d) shows the transition response from stand-alone to grid-connected mode. During stand-alone mode, the microgrid was formed by one UPS unit supplying 60kW resistive load. When the grid becomes available, the STS closes and reconnects the microgrid seamlessly to the grid. Only small fluctuations appear on the DC-link which settles within two fundamental cycles. The load current sees a small increase due to the fact that the grid voltage is slightly higher than the stand-alone UPS voltage because of the inherit characteristic of the voltage droop control. The UPS current starts to decrease and will eventually become equivalent to the power command in grid-connected mode. Fig. 13(e) shows the transient response when the active power demand $P_{ref}$ changes from -10kW to 60kW by the user interface. The controller ramps up the power demand gradually (to avoid any unnecessary transient as discussed earlier) and thus the current changes amplitude and phase gradually. The DC-link voltage drops from 800V (controlled by the AC/DC active rectifier) to 750V (controlled by the DC/DC converter). Fig. 13(f) shows the DC-link voltage controller transient response during transition from battery discharging mode (the DC-link voltage is controlled by the DC/DC convertor) to battery charging mode (the DC-link voltage is controlled by the AC/DC converter). The DC-link shows good transient response similar to the simulated response shown in Fig. 11. Fig. 19 shows the starting sequence of one UPS unit in grid-connected mode.

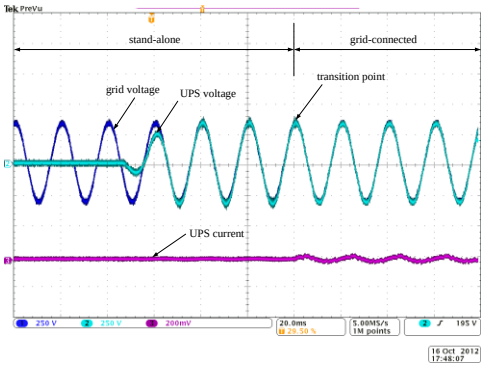


Fig. 14. UPS and grid voltages during transition from stand-alone mode to grid-connected mode.

Initially, the inverter voltage is controlled to have the same magnitude and frequency as the grid voltage and it is also synchronised so the power angle is minimised to be virtually zero. When the STS controller is satisfied that the two voltage signals across its terminals are healthy and in phase it closes the STS so the microgid is connected to the main grid.

## VI. Conclusion

A line interactive UPS system to be used in microgrids has been presented. The control strategy that is based on voltage and frequency drooping technique was demonstrated experimentally to be capable of achieving seamless transfer between grid connected and stand-alone parallel modes of operation. A DC-link voltage controller that sets the active power demand during battery charging mode was demonstrated to be effective in facilitating smooth transition between battery charging and discharging modes.

## References

[1] J. C. Wu and H. L. Jou, "A new UPS scheme provides harmonic suppression and input power factor correction," *IEEE Trans. Ind. Electron.*, vol. 42, no. 6, pp. 629–635, Dec. 1995.

[2] Y. Lin, G. Joos, and J. F. Lindsay, "Performance analysis of parallel processing UPS systems," in *Proc. IEEE Applied Power Electronics Conf. and Expo.*, Mar. 1993, pp. 533–539.

[3] F. Kamran and T. G. Habetler, "A novel on-line UPS with universal filtering capabilities," *IEEE Trans. Power Electron.*, vol. 13, no. 3, pp. 410–418, May 1998.

[4] S. A. O. da Silva, P. F. Donoso-Garcia, P. C. Cortizo, and P. F. Seixas, "A three-phase line-interactive UPS system implementation with series-parallel active power-line conditioning capabilities," *IEEE Trans. Ind. Appl.*, vol. 38, no. 6, pp. 1581–1590, Nov./Dec. 2002

[5] B. H. Kwon, J. H. Choi, and T. W. Kim, "Improved single-phase line-interactive UPS," *IEEE Trans. Ind. Electron.*, vol. 48, no. 4, pp. 804–811, Aug. 2001.

[6] F. Barrero, S. Martinez, F. Yeves, F. Mur, and P. M. Martinez, "Universal and reconfigurable to UPS active power filter for line conditioning," *IEEE Trans. Power Del.*, vol. 18, no. 1, pp. 283–290, Jan. 2003.

[7] C.-C. Yeh and M. D. Manjrekar, "A reconfigurable uninterruptible power supply system for multiple power quality applications," *IEEE Trans. Power Electron.*, vol. 22, no. 4, pp. 1361–1372, Jul. 2007.

[8] R. Tirumala, N. Mohan, and C. Henze, "Seamless transfer of grid connected PWM inverters between utility-interactive and stand-alone modes," in *Proc. IEEE APEC*, Dallas, TX, Mar. 2002, pp. 1081–1086.

[9] F.S. Pai, and S. J. Huang, "A novel design of line-interactive uninterruptible power supplies without load current sensors," IEEE Trans. Power Electron, vol. 21, no. 1, pp. 202-210, Jan. 2006.

[10] H. Tao, J. L. Duarte, and M. A. M. Hendrix, "Line-interactive UPS using fuel cell as the primary source," *IEEE Trans. Ind. Electron.*, vol. 55, no. 8, pp. 3005–3011, Aug. 2008.

[11] M. Arias, A. Fernandez, D. G. Lamar, M. Rodriguez, and M. M. Hernando, "Simplified voltage-sag filler for line-interactive uninterruptible power supplies," *IEEE Trans. Ind. Electron.*, vol. 55, no. 8, pp. 3005–3011, Aug. 2008.

[12] H. Kim, T. Yu, and S. Choi, "Indirect Current Control Algorithm for Utility Interactive Inverters in Distributed Generation Systems," *IEEE Trans. Power Electron*, vol. 23, no. 3, pp. 1342-1347, May. 2008.

[13] W.J. Ho, J.B. Lio, and W.S. Feng, "A line-interactive UPS structure with built-in vector-controlled charger and PFC," in *Proc. Int. Conf. Power Electronics and Drive Systems*,1997, pp. 127-132.

[14] Y. Okui, S. Ohta, N. Nakamura, H. Hirata, and M. Yanagisawa, "Development of line interactive type UPS using a novel control system," in *Proc. IEEE Int. Telecommunication Energy Conf.*, 2003, pp. 796–801.

[15] M. Chandorkar, D. Divan, Y. Hu, and B. Banerjee, "Novel architectures and control for distributed ups systems," in *Applied Power Electronic Conference and Exposition*, vol. 2, February 1994, pp. 683–689.

[16] J. M. Guerrero, J. C. Vasquez, J. Matas, M. Castilla, and L.G. de Vicuna, "Control Strategy for Flexible Microgrid Based on Parallel Line-Interactive UPS Systems," *IEEE Trans. Ind. Electron.*, vol. 26, no. 3, pp. 726–736, Mar. 2009.

[17] R. M. Kamel, A. Chaouachi, and K. Nagasaka, "Three control strategies to improve the microgrid transient dynamic response during isolated mode: a comparative study," *IEEE Trans. Ind. Electron.*, vol. 60, no. 4, pp. 1314-1322, Apr. 2013.

[18] J. M. Guerrero, L. G. de Vicuña, J. Matas, M. Castilla, and J. Miret, "Output Impedance Design of Parallel-Connected UPS Inverters With Wireless Load-Sharing Control," *IEEE Trans. Ind. Electron.*, vol. 52, no. 4, pp. 1126-1135, Aug. 2005.

[19] M. Savaghebi, A. Jalilian, J. C. Vasquez, and J. M. Guerrero, "Autonomous voltage unbalance compensation in an islanded droop-controlled microgrid," *IEEE Trans. Ind. Electron.*, vol. 60, no. 4, pp. 1390-1402, Apr. 2013.

[20] J. C. Vasquez, J. M. Guerrero,M. Savaghebi, J. Eloy-Garcia, and R. Teodorescu, "Modeling, analysis, and design of stationary-reference-frame droop-controlled parallel three-phase voltage source inverters," *IEEE Trans. Ind. Electron.*, vol. 60, no. 4, pp. 1271-1280, Apr. 2013.

[21] IEEE Standard for Interconnecting Distributed Resources with Electric Power Systems, *IEEE Standard 1547, 2003*.

**Mohammad A. Abusara** received the B.Eng. degree from Birzeit University, Palestine, in 2000, and the Ph.D. degree from the University of Southampton, U.K, in 2004, both in electrical engineering. From 2003 to 2010, he was with Bowman Power Group, Southampton, UK, responsible for research and development of digital control of power electronics for distributed energy resources, hybrid vehicles, and machines and drives.. He is currently a Lecturer in Renewable Energy at the University of Exeter, U.K.

**Josep M. Guerrero** (S'01–M'04–SM'08) received the B.S. degree in telecommunications engineering, the M.S. degree in electronics engineering, and the Ph.D. degree in power electronics from the Technical University of Catalonia, Barcelona, Spain, in 1997,2000, and 2003, respectively He is a Full Professor at the Department of Energy Technology, Aalborg University, Aalborg East, Denmark. His research interests include power electronics converters for distributed generation and distributed energy storage systems, control and management of microgrids and islanded minigrids, and photovoltaic and wind power plants control.

**Suleiman M. Sharkh** received the B.Eng. and Ph.D degrees in electrical engineering from the University of Southampton, Southampton, U.K., in 1990 and 1994, respectively. He is currently a Senior Lecturer and the head of the Electro-Mechanical Research Group at the University of Southampton. Dr. Sharkh is a member of the IET and a Chartered Engineer. He was the 2008 winner of The Engineer Energy Innovation Award for his work on rim driven thrusters and marine turbine generators.